ELSEVIER

Chemical Geology 177 (2001) 381–397

CHEMICAL GEOLOGY
INCLUDING
ISOTOPE GEOSCIENCE

www.elsevier.com/locate/chemgeo

Pb diffusion in Cr diopside, augite, and enstatite, and consideration of the dependence of cation diffusion in pyroxene on oxygen fugacity

D.J. Cherniak *

Department of Earth and Environmental Sciences, Rensselaer Polytechnic Institute, 110 8th Street, Science Center, Troy, NY 12180-3590, USA

Received 2 March 2000; accepted 28 November 2000

Abstract

Chemical diffusion of Pb under anhydrous, pO_2-buffered conditions has been measured in natural pyroxenes of three different compositions: a chromian diopside, an augitic clinopyroxene, and a near-end member enstatite. Sources of diffusant consisted of PbS powder and ground pyroxene mixed together, pre-reacted in evacuated silica capsules at 1050°C, and re-ground. Prepared sample capsules were annealed for times ranging from several hours to a few months, at temperatures from 850°C to 1050°C. The Pb distributions in the pyroxene specimens were profiled by Rutherford Backscattering Spectrometry (RBS).

The following Arrhenius relations are obtained for Pb diffusion in the pyroxenes when buffered at QFM:

$$D_C = 8.7 \times 10^{-7} \exp(-351 \pm 36\,\mathrm{kJ\,mol^{-1}}/RT)\ \mathrm{m^2\,s^{-1}}. \quad (\text{Cr diopside})$$

$$D_A = 3.8 \times 10^{-5} \exp(-372 \pm 15\,\mathrm{kJ\,mol^{-1}}/RT)\ \mathrm{m^2\,s^{-1}}. \quad (\text{augite})$$

$$D_E = 6.6 \times 10^{-7} \exp(-366 \pm 29\,\mathrm{kJ\,mol^{-1}}/RT)\ \mathrm{m^2\,s^{-1}}. \quad (\text{enstatite})$$

In all cases, diffusion is measured perpendicular to the *c*-axis. Diffusion in Cr diopside does not appear to be strongly anisotropic, as diffusion rates for transport parallel to *c* are similar to the (110) results above. Diffusion in the augite is faster (by nearly an order of magnitude) than Pb diffusion in the Cr diopside. Diffusion tends to be faster in pyroxenes with higher iron contents as was evident in our earlier work (Chemical Geology 150 (1998a) 105), but simple correlations are not obvious. Pb diffusion in enstatite is considerably slower than in the clinopyroxene compositions studied.

To investigate the fO_2 dependence of Pb diffusion in pyroxene, experiments using the Cr diopside, augite, and enstatite, as well as the near end-member diopside and a more iron rich clinopyroxene employed in a recent diffusion study (Chemical Geology 150 (1998a) 105), were run at 950°C under oxygen fugacities ranging from 10^{-6} to 10^{-16}. All of the pyroxenes exhibited a positive dependence of Pb diffusion rate on fO_2, with values of *m* ranging from 0.14 to 0.20, given

* Fax: +1-518-276-6680.
E-mail address: chernd@rpi.edu (D.J. Cherniak).

PII: S0009-2541(00)00421-6

$D \propto (fO_2)^m$. Interestingly, the exponential term for diopside is 0.19, in good agreement with the value $+3/16$ determined from point defect models for diffusion mechanisms controlled by cation vacancies (J. Geophys. Res. 99 (1994) 9423).

The activation energies for Pb diffusion in all of the pyroxenes studied are relatively high, and Pb diffusivities slow when compared with the extant diffusion data for most other minerals. It follows, as consequence of these comparatively slow diffusivities, that Pb closure temperatures are higher in pyroxenes than for the majority of minerals, with the exception of a few phases such as zircon, monazite, and garnet. The slightly faster diffusivities that characterize Fe-rich clinopyroxenes will lead to somewhat depressed closure temperatures, but pyroxenes in general should be fairly retentive of Pb isotopic information when subjected to all but the most extreme thermal events.

Keywords: Diffusion; Pyroxene; Oxygen fugacity; Lead; Rutherford backscattering

1. Introduction

Pyroxenes, given their ubiquity, are a ferromagnesian silicate phase of extreme geologic importance. Because of their common occurrence and ability to incorporate large divalent cations (such as Pb) on M-sites, various pyroxenes can play an important role in Pb isotope systematics. In order to better understand these systematics and interpret the isotopic record, the determination of Pb diffusion rates for the broadest range of minerals incorporating Pb is warranted.

In this paper, Pb diffusion is measured in natural pyroxenes of three different compositions: a chromian diopside, an augitic pyroxene, and a near-end-member enstatite. The work reported here is a continuation of investigation into Pb diffusion in various pyroxene compositions (begun in Cherniak, 1998a), in efforts to assess the influence of crystal–chemical parameters on diffusion in pyroxenes. To attain a broader perspective, we compare the present results with the extant Pb diffusion data for other minerals and evaluate how well findings for pyroxenes conform to models that predict diffusion behavior as the function of crystal–chemical parameters, and also consider the findings with respect to diffusion of other species in pyroxene in order to better understand the processes influencing and controlling cation exchange.

We explore as well the dependence of Pb diffusion rates on oxygen fugacity in these three pyroxene compositions, along with those pyroxenes studied in an earlier paper on Pb diffusion (Cherniak, 1998a). Since natural pyroxenes commonly contain Fe and other transition elements, their defect chemistries can be strongly affected by ambient fO_2, and this in turn can influence diffusion rates and mechanisms. The dependence (or, as the case may be, lack thereof) of Pb diffusion rates on fO_2 thus offers insight into the dominant mechanisms governing Pb diffusion in pyroxenes, and, coupled with information on the dependence of Pb diffusion on pyroxene composition, permits us to assess the utility of the data in describing diffusional behavior in natural systems.

2. Experimental procedure

The minerals used in this study were an augitic pyroxene from Templeton, Quebec Province, obtained from the Smithsonian's collection (specimen number R15162-1), a chromian diopside (from an unknown locality) and a near-end member enstatite from Embilipitiya, Sri Lanka, obtained from the Harvard University collection (specimen #131539). The enstatite crystals were glass-clear. The chromian diopside crystals were a clear bright green, while the augitic pyroxene was a deeper green in color. A few experiments were also conducted on a near-end-member diopside from DeKalb, New York ($\sim Di_{95}$), and another clinopyroxene of higher iron content (with $\sim$ 40% diopside component, referred to in the subsequent text as "MBB cpx"), in which Pb diffusion has previously been measured under QFM- and "self-buffered" conditions (Cherniak, 1998a), in order to more fully investigate the dependence of Pb diffusion rates on oxygen fugacity. Compositional information for these pyroxenes is presented in Table 1.

Specimens of the augitic pyroxene, chromian diopside, and enstatite (as well as the two other pyroxenes) were cleaved along dominant cleavage planes ({210} for the enstatite, {110} for the others) and underwent no further surface preparation. In

Table 1
Compositional information on pyroxenes used in this study

	Cr diopside	Augite	Enstatite	DeKalb Di	MBB cpx
Wt.% oxides, from electron microprobe analyses					
SiO_2	55.28	55.08	60.03	55.06	51.02
TiO_2	0.07	–	0.02	–	–
Al_2O_3	0.22	0.75	1.19	0.55	–
FeO	1.18	3.91	0.59	0.99	16.49
MnO	0.08	0.18	–	–	1.81
MgO	17.75	15.43	38.94	17.58	6.89
CaO	24.63	24.75	0.04	25.23	23.88
Cr_2O_3	0.65	–	–	–	–
Na_2O	0.47	0.39	–	0.52	–
Total	100.33	100.49	100.81	99.93	100.09
Cations on basis of six oxygens					
Si	2.00	2.00	1.99	1.99	2.00
Al	0.01	0.03	0.05	0.02	–
Fe	0.04	0.12	0.02	0.03	0.54
Mn	–	0.01	–	–	0.06
Mg	0.96	0.84	1.93	0.95	0.40
Ca	0.95	0.96	–	0.98	1.00
Cr	0.02	–	–	–	–
Na	0.03	0.03	–	0.03	–

addition, some specimens of the Cr diopside were cut perpendicular to the *c*-axis and polished to 0.05 μm alumina. All samples were cleaned ultrasonically in distilled water and ethanol and then pre-annealed under buffered conditions using solid buffers (either IW, QFM, or MH, depending on conditions of subsequent diffusion anneals) for 48 h at 950°C to anneal possible surface damage produced by cold-working of the polished samples, and to equilibrate point defects to conditions that would be similar to those experienced during the experiments.

The sources of Pb for the experiments were mixtures of PbS powder and finely ground pyroxene (of the same composition as the samples) in 4:1 (by weight) ratio. The PbS–pyroxene mixtures were loaded into silica capsules and sealed under vacuum. The silica capsules were heated at 1050°C for 24 h. The mixtures were then finely ground for use as the source of diffusant. The experiments themselves were conducted using double silica glass capsules (Cherniak, 1998a). The sample and source were placed in an open silica glass capsule (~1 cm long and 5 mm o.d.); the open capsule was placed in a larger (several cm long, 6 mm i.d., 8 mm o.d.) silica glass capsule containing a solid buffer. A silica glass plug was placed in the larger glass tube and the assembly sealed under vacuum.

Prepared sample capsules were annealed in 1-atm furnaces at temperatures from 850°C to 1100°C for times ranging from a few hours to 3 months. "Zero-time" experiments were also run at 1000°C and 950°C for enstatite and augitic pyroxene, respectively. For these experiments, the sample capsules were prepared as above for the QFM buffered an-

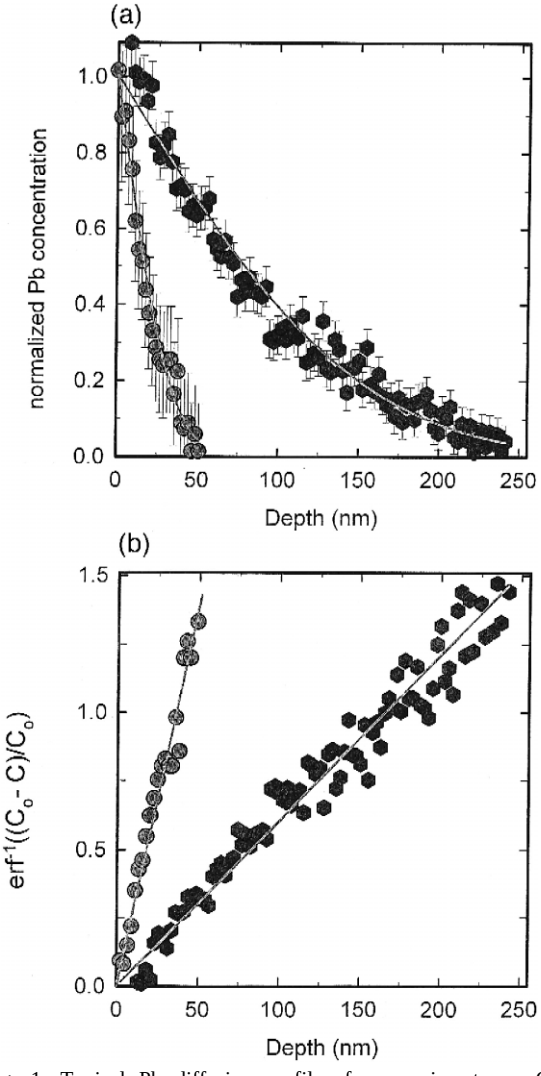

Fig. 1. Typical Pb diffusion profiles for experiments on Cr diopside and augitic pyroxene. In (a), the measured diffusion profiles are plotted with complementary error function curves. In (b), the data are linearized by inversion through the error function. Slopes of the lines are equal to $(4Dt)^{-1/2}$.

neals. The samples were placed in the furnace, brought up to run temperature, and immediately quenched. Temperatures in the 800–1050°C experiments were monitored with type K (chromel–alumel) thermocouples during the course of the anneals; temperature uncertainties are ±2°C. A type S (Pt–Pt10%Rh) thermocouple was used for the 1100°C runs, with comparable temperature uncertainty. On completion of the anneals, samples were quenched merely by removing them from furnaces and permitting them to cool in air. Samples were then removed from capsules, freed of residual source material and cleaned ultrasonically in successive baths of dilute HCl (~4N), distilled water, and ethanol. The enstatite was cleaned ultrasonically in distilled water and ethanol only. The samples were readily removed from the source material and sample surfaces using these sources are easily cleaned of the residual (Cherniak, 1998a).

3. RBS analysis

RBS has been used in recent work on Ca self-diffusion and Pb chemical diffusion in diopside (Dimanov et al., 1996; Dimanov and Ingrin, 1995; Cherniak, 1998a), in an earlier study of Sr diffusion in diopside (Sneeringer et al., 1984), and in many other diffusion studies (e.g., Cherniak and Watson, 1992, 1994; Cherniak, 1995a). The experimental and

Table 2
Pb diffusion in augite and Cr diopside

	T (°C)	Time (s)	D (m^2 s^{-1})	log D	±	Buffer
Augite						
QUAPb-6	850	5.20×10^6	8.10×10^{-23}	−22.09	0.26	QFM
QUAPb-3	902	2.24×10^6	7.75×10^{-22}	−21.11	0.09	QFM
QUAPb-1	933	1.11×10^6	4.61×10^{-21}	−20.34	0.06	QFM
QUAPb-2	950	6.26×10^5	5.69×10^{-21}	−20.25	0.06	QFM
QUAPb-12	950	3.20×10^5	6.87×10^{-20}	−19.16	0.08	MH
QUAPb-11	950	6.55×10^5	4.32×10^{-22}	−21.36	0.17	IW
QUAPb-7	998	7.60×10^5	1.51×10^{-20}	−19.82	0.07	QFM
QUAPb-8	1000	4.10×10^5	1.66×10^{-20}	−19.78	0.08	QFM
QUAPb-9	1000	8.28×10^4	2.23×10^{-20}	−19.65	0.08	QFM
QUAPb-4	1002	1.78×10^5	5.43×10^{-20}	−19.27	0.07	QFM
QUAPb-5	1050	5.76×10^4	1.03×10^{-19}	−18.99	0.09	QFM
Cr Diopside diffusion normal to c						
CrDiPb-3a	850	6.71×10^6	6.89×10^{-23}	−22.16	0.25	QFM
CrDiPb-1a	900	2.40×10^6	1.34×10^{-22}	−21.87	0.21	QFM
CrDiPb-2a	950	9.72×10^5	4.39×10^{-22}	−21.36	0.28	QFM
CrDiPb-8a	950	9.58×10^5	1.35×10^{-20}	−19.87	0.06	MH
CrDiPb-7a	1000	9.00×10^4	4.14×10^{-21}	−20.38	0.19	QFM
CrDiPb-4a	1000	2.30×10^5	3.26×10^{-21}	−20.49	0.27	QFM
CrDiPb-5a	1000	7.78×10^5	3.59×10^{-21}	−20.45	0.10	QFM
CrDiPb-9a	1050	8.64×10^4	1.20×10^{-20}	−19.92	0.18	QFM
Diffusion parallel to c						
CrDiPb-3a	850	6.71×10^6	7.50×10^{-23}	−22.13	0.29	QFM
CrDiPb-1c	900	2.40×10^6	3.86×10^{-22}	−21.42	0.29	QFM
CrDiPb-2c	950	9.72×10^5	1.02×10^{-21}	−20.99	0.15	QFM
CrDiPb-8a	950	9.58×10^5	9.63×10^{-21}	−20.02	0.20	MH
CrDiPb-10	950	8.64×10^5	1.45×10^{-22}	−21.84	0.21	IW
CrDiPb-7c	1000	9.00×10^4	3.16×10^{-21}	−20.50	0.26	QFM
CrDiPb-4c	1000	2.30×10^5	1.84×10^{-21}	−20.74	0.18	QFM
CrDiPb-5c	1000	7.78×10^5	4.44×10^{-21}	−20.35	0.05	QFM
CrDiPb-9c	1050	8.64×10^4	6.77×10^{-21}	−20.17	0.27	QFM

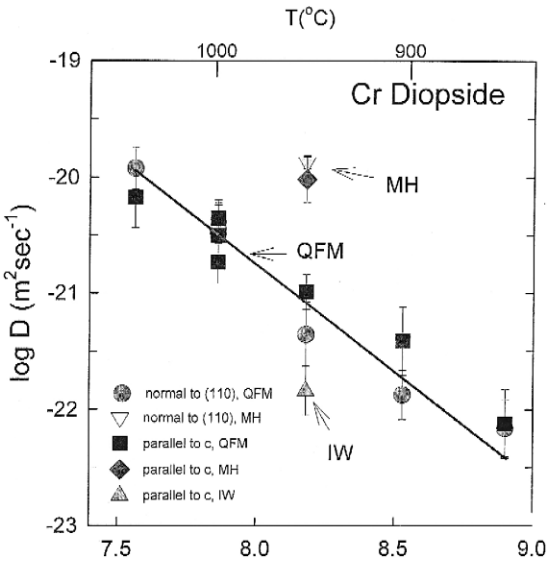

Fig. 2. Arrhenius plot of Pb diffusion data for chromian diopside, for diffusion normal and parallel to c under a range of fO_2 conditions, from magnetite–hematite (MH) to iron–wüstite (IW). The line is a least-squares fit to the diffusion data for transport normal to c buffered at QFM. For diffusion normal to c, an activation energy 351 kJ mol^{-1} and pre-exponential factor 8.66×10^{-7} m^2 s^{-1} are obtained. For transport parallel to c, an activation energy of 309 kJ mol^{-1} and pre-exponential factor 2.00×10^{-8} m^2 s^{-1} are determined. Anisotropy in Pb diffusion is not pronounced. Diffusion under more oxidizing conditions is faster than diffusion under conditions more reducing than QFM.

analytical approach used here is similar to that used in our previous work. Helium beam energies used ranged between 1 and 2 MeV, with incident energies in the lower range used in some analyses of the enstatite and chromian diopside in order to improve sensitivity. Spectra were converted to Pb concentration profiles employing procedures outlined in publications cited above. The code used to extract depth scales from the raw data took into account the compositional (and density) differences of the pyroxenes employed in this study and the effect of this variation on stopping powers for the helium ions. The resultant profiles (concentration vs. depth) were fit with a model to determine the diffusion coefficient (D). Diffusion is modeled as simple one-dimensional, concentration independent diffusion in a semi-infinite medium with a source reservoir maintained at constant concentration (i.e., a complementary error function solution). The rationale for the use of this model has been elsewhere addressed (e.g., Cherniak and Watson, 1992, 1994; Cherniak, 1993). Diffusivities are evaluated by plotting the inverse of the error function (i.e., $\mathrm{erf}^{-1}((C_0 - C(x,t))/C_0)$) vs. depth ($x$) in the sample. A straight line of slope $(4Dt)^{-1/2}$ results if the data satisfy the conditions of the model. C_0, the surface concentration of diffusant, is independently determined by iteratively varying its value until the intercept of the line converges on zero. In Fig. 1, typical diffusion profiles and their inversions through the error function are shown. The uncertainties in concentration and depth from each data point (mainly derived from counting statistics in the former and detector resolution in the latter) were used to evaluate the uncertainties in the diffusivities determined from the fits to the model.

4. Results

The results for the Pb diffusion anneals of the chromian diopside are presented in Table 2 and

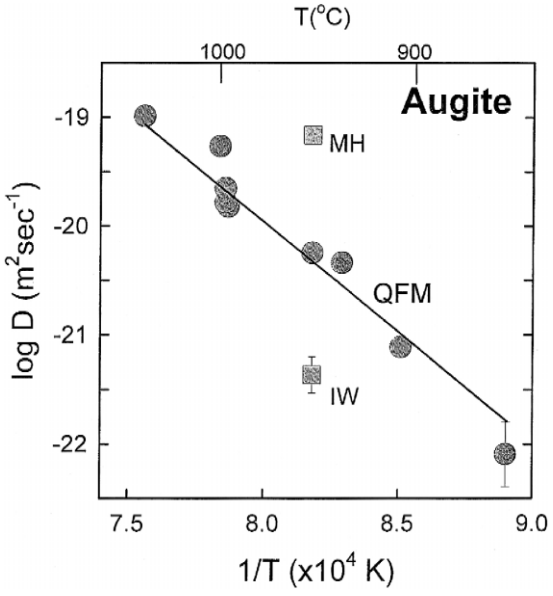

Fig. 3. Arrhenius plot for Pb diffusion in augitic pyroxene. From a fit to the diffusion data, we obtain an activation energy of 372 kJ mol^{-1} and pre-exponential factor 3.78×10^{-5} m^2 s^{-1} for diffusion anneals buffered at QFM. Pb diffusion in systems buffered at MH is about an order of magnitude faster than diffusion in systems buffered at QFM, while diffusion under conditions more reducing (IW) is an order of magnitude slower.

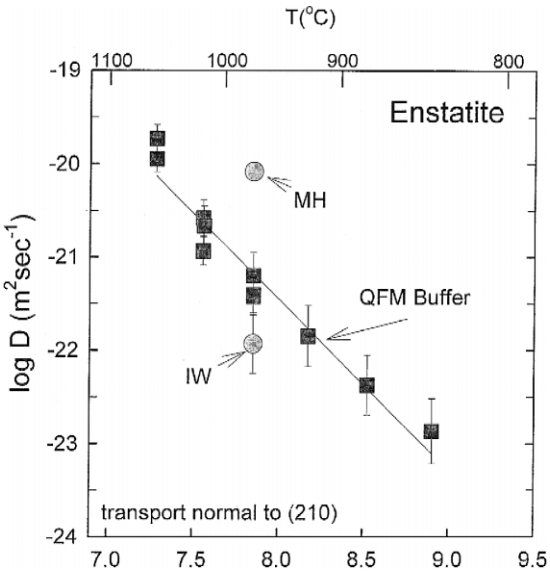

Fig. 4. Arrhenius plot of Pb diffusion data for enstatite. From the least-squares fit to the diffusion data, an activation energy of 366 kJ mol^{-1} and pre-exponential factor 6.63×10^{-7} m^2 s^{-1} for diffusion anneals buffered at QFM are obtained. Again, a positive dependence of Pb diffusion on fO_2 can be observed.

plotted in Fig. 2. For the QFM buffered experiments with transport normal to the {110} cleavage plane, an activation energy 351 ± 36 kJ mol^{-1} (83.9 ± 8.6 kcal mol^{-1}) and pre-exponential factor 8.66×10^{-7} m^2 s^{-1} ($\log D_0 = -6.06 \pm 1.49$) are obtained. For transport parallel to *c*, an activation energy of 309 ± 40 kJ mol^{-1} (73.9 ± 9.6 kcal mol^{-1}) and pre-exponential factor 2.00×10^{-8} m^2 s^{-1} ($\log D_0 = -7.70 \pm 1.67$) are determined. Little anisotropy is noted in investigating these two orientations, a finding consistent with observations from other studies of cation diffusion in pyroxenes (e.g., Cherniak, 1998a; Schwandt et al., 1998; Sneeringer et al., 1984). A fit to data for both orientations yields the values 336 ± 27 kJ mol^{-1} (80.3 ± 6.4 kcal mol^{-1}) for the activation energy and 2.36×10^{-7} m^2 s^{-1} ($\log D_0 = -6.63 \pm 1.10$) for the pre-exponential factor.

The results for experiments on the augitic pyroxene are presented in Table 2 and plotted in Fig. 3. For transport normal to (110) under QFM-buffered conditions, the activation energy 372 ± 15 kJ mol^{-1} (89 ± 4 kcal mol^{-1}) and the pre-exponential factor 3.78×10^{-5} m^2 s^{-1} ($\log D_0 = -4.42 \pm 0.64$) are found.

Results for diffusion measurements on the enstatite are plotted in Fig. 4 and presented in Table 3. An activation energy of 366 ± 29 kJ mol^{-1} ($87.4 \pm$

Table 3
Pb diffusion in enstatite, DeKalb diopside and MBB cpx

	T (°C)	Time (s)	*D* (m^2 s^{-1})	log *D*	±	Buffer
Enstatite						
EnPb-9	850	7.68×10^{6}	1.41×10^{-23}	−22.85	0.29	QFM
EnPb-6	900	3.28×10^{6}	4.29×10^{-23}	−22.37	0.32	QFM
EnPb-5	950	1.83×10^{6}	1.42×10^{-22}	−21.85	0.33	QFM
EnPb-7	1000	5.20×10^{5}	3.75×10^{-22}	−21.43	0.20	QFM
EnPb-8	1000	1.71×10^{5}	6.23×10^{-22}	−21.21	0.27	QFM
EnPb-10	1000	1.00×10^{6}	3.88×10^{-22}	−21.41	0.19	QFM
EnPb-12	1000	9.43×10^{5}	1.17×10^{-22}	−21.93	0.31	IW
EnPb-13	1000	2.59×10^{5}	8.27×10^{-21}	−20.08	0.06	MH
EnPb-11	1049	9.54×10^{4}	2.15×10^{-21}	−20.67	0.22	QFM
EnPb-3	1050	2.48×10^{5}	1.15×10^{-21}	−20.94	0.15	QFM
EnPb-2	1100	3.00×10^{4}	1.13×10^{-20}	−19.95	0.14	QFM
EnPb-4	1100	1.08×10^{4}	1.85×10^{-20}	−19.73	0.15	QFM
DeKalb diopside, diffusion normal to c						
DKDPb-29	950	7.79×10^{5}	2.79×10^{-20}	−19.55	0.05	MH
DKDPb-30	950	7.81×10^{5}	4.76×10^{-22}	−21.32	0.21	IW
MBB clinopyroxene (~ Di_{40}), diffusion normal to c						
MBBPb-16	950	7.92×10^{5}	3.38×10^{-20}	−19.74	0.11	MH
MBBPb-15	950	7.96×10^{5}	7.92×10^{-22}	−21.10	0.20	IW

7.0 kcal mol^{-1}), and pre-exponential factor of 6.63 $\times 10^{-7}$ m^2 s^{-1} (log $D_0 = -6.18 \pm 1.18$) are determined for transport normal to (210) under QFM-buffered conditions.

Findings from experiments run on these pyroxenes under both more oxidizing and more reducing conditions are also plotted in Figs. 2–4, and included in Tables 2 and 3. Results from experiments run under these conditions on the DeKalb diopside and the MBB cpx are plotted in Fig. 5, along with the Arrhenius relations reported in Cherniak (1998a) for Pb diffusion in these pyroxenes under QFM buffered conditions, as well as the Arrhenius line for Pb diffusion in diopside under "self-buffered" conditions (Cherniak, 1998a). In all cases, there is a positive dependence of Pb diffusion rates on fO_2. This is clearly shown in Fig. 6, where log D_{Pb} at constant temperature (1000°C for the enstatite, 950°C for other pyroxenes) for all pyroxene compositions is plotted as a function of log fO_2. The slopes of these lines, presented in Table 4, are all similar, ranging from 0.141 to 0.203. Comparison of the Arrhenius relation for Pb diffusion in DeKalb diopside under

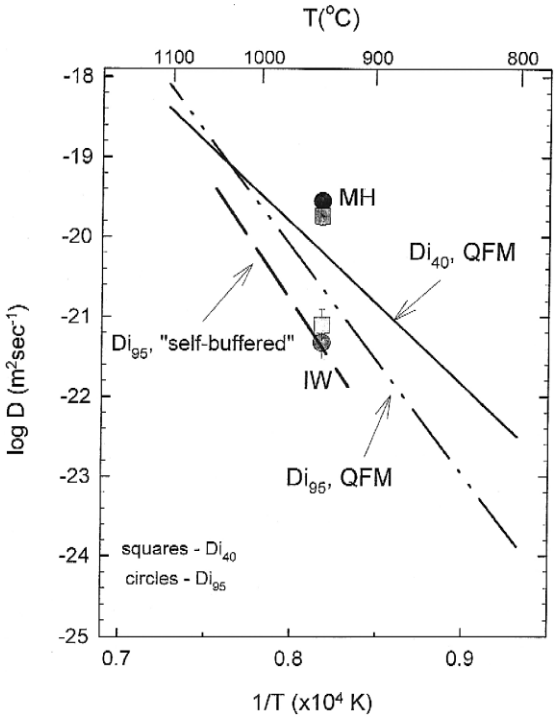

Fig. 5. Plot of Pb diffusion in MBB cpx (Di_{40}) and DeKalb diopside (Di_{95}). Lines are Arrhenius relations from Cherniak (1998a) for Pb diffusion in these clinopyroxenes in experiments buffered at QFM. The symbols (circles for Di_{95}, squares for Di_{40}) are measurements made in the present study of Pb diffusion in these pyroxenes under buffered conditions more reducing (IW) and more oxidizing (MH) than QFM. The same trends of increasing diffusion rates with increasing fO_2 are noted here. The similarity of diffusion rates for the IW-buffered DeKalb diopside and the "self-buffered" anneals of Cherniak (1998a), suggests that the "self-buffered" system is a reducing environment.

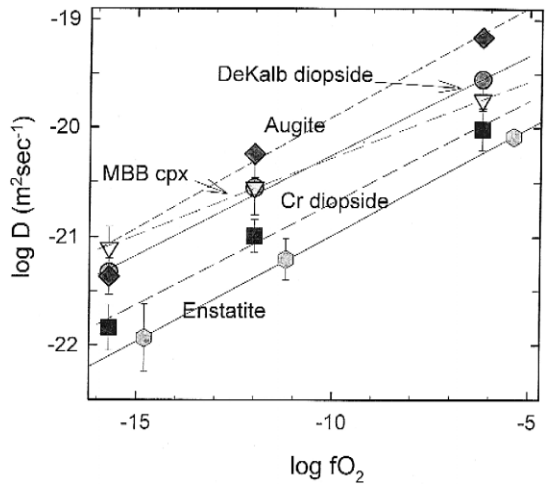

Fig. 6. Dependence of diffusion rates on fO_2. Diffusivities at fixed temperature (1000°C for the enstatite, 950°C for other pyroxenes) for all pyroxene compositions are plotted as a function of log fO_2. The slopes of these lines (Table 4) are all positive and have similar values, ranging from 0.141 to 0.203. The sign and range of values of this parameter m (where $D \propto (pO_2)^m$) is quite similar to the value of $+3/16$ ($=0.188$) derived from a point defect model for diopside (Jaoul and Raterron, 1994) for a vacancy-controlled (octahedrally coordinated vacancies) mechanism for diffusion.

Table 4
Dependence of Pb diffusion on oxygen fugacity for several pyroxene compositions. The table includes values for the exponent m, where $D \propto (pO_2)^m$. The point defect model proposed by Jaoul and Raterron (1994) for diopside predicts an exponent of $+3/16$ (i.e., 0.188) for vacancy controlled diffusion

	m
DeKalb diopside	0.183 ± 0.021
MBB clinopyroxene	0.141 ± 0.020
Cr diopside	0.188 ± 0.030
Quebec augite	0.203 ± 0.014
Enstatite	0.200 ± 0.019

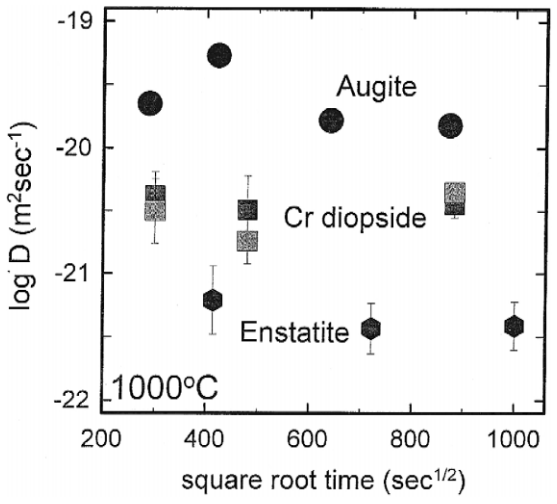

Fig. 7. Time series for Pb diffusion in enstatite, augite and Cr diopside (both orientations). All experiments were run at 1000°C and buffered at QFM. Diffusion rates for a given pyroxene are quite similar, despite differences in anneal times ranging over about an order of magnitude, suggesting that the dominant process being measured is volume diffusion.

"self-buffered" conditions (Cherniak, 1998a) with diffusivities found under controlled buffered conditions (Fig. 5) suggests that the "self-buffered" system (with its relatively iron-poor natural diopside) is more reducing than QFM, in contrast to the conclusion drawn in Cherniak (1998a).

I performed both "zero-time" experiments on the augitic pyroxene and the enstatite, and time-series studies at 1000°C in order to verify that the measured concentration profiles represent volume diffusion and are not a result of other phenomena such as surface reaction that may otherwise result in enhanced Pb yields in the near-surface region. The "zero-time" anneal also serves to highlight possible systematic problems in the experimental approach. In Fig. 7, the results of the time series at 1000°C for the Cr diopside (in both orientations), the augitic pyroxene, and the enstatite are plotted. Diffusivities for a given pyroxene are quite similar for times ranging over more than an order of magnitude, suggesting that volume diffusion is the dominant contributor to the observed diffusion profiles. However, there are clear differences in the magnitudes of diffusivities among the different pyroxene compositions, with Pb diffusion in the augitic pyroxene the fastest, followed next by the Cr diopside, with diffusion in the enstatite the slowest. The zero-time experiments (not plotted) display little evidence of significant near-surface Pb during the heat-up and quench phases of the anneal, offering further confirmation that Pb profiles are a consequence primarily of lattice diffusion.

5. Discussion

5.1. Effects of pyroxene composition on diffusion rates

A summary of Pb diffusion for pyroxenes under QFM-buffered conditions is plotted in Fig. 8. Activation energies for Pb diffusion in these pyroxenes are similar ($\sim$ 390–350 kJ mol^{-1}), with the exception of the DeKalb diopside, which has a higher value. Dimanov et al. (1996) have found a positive correlation between Ca diffusion rates and Fe content in diopside, with diffusion differing by nearly a log unit

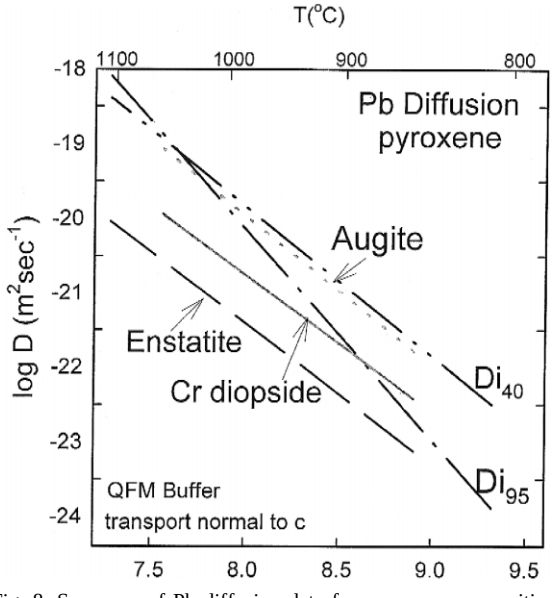

Fig. 8. Summary of Pb diffusion data for pyroxene compositions investigated in this work and those from Cherniak (1998a). Diffusion in clinopyroxenes of higher Fe content is faster than in Fe-poor specimens. Pb diffusion in enstatite is slower than diffusion in the clinopyroxene compositions investigated. Activation energies for diffusion, with the exception of the DeKalb diopside (Di_{95}) are similar.

between diopsides with 0.4 and 2.4 at.% Fe, when the data are "normalized" to constant pO_2 and T. Activation energies for Ca diffusion in these diopsides were, however, found to be quite similar. In the case of Pb diffusion, comparable trends may broadly apply. We do note that the more iron-rich pyroxenes do exhibit somewhat faster Pb diffusivities, but simple correlations are precluded both because of the broad range of Fe concentrations spanned in the investigated specimens, and because, obviously, not all of the samples are diopsides (or even clinopyroxenes).

Clearly, diffusion is affected by defect chemistry; it is certainly likely that the differences in major and minor element concentrations and variations in defect populations between the pyroxenes have significant effects on diffusion, although the similarities in fO_2 dependence on Pb diffusion rates among the pyroxenes suggest a common controlling defect mechanism. This will be further discussed in subsequent sections.

The pronounced compositional differences among the pyroxenes used in our investigation lead to significant differences in crystal–chemical properties that may substantially influence diffusivities. Dahl (1997) has shown that there is some correlation between mineral ionic porosity (i.e., the "free space" in a crystal unoccupied by anions or cations; cf. Fortier and Giletti, 1989; Dowty, 1980) and Pb diffusivities; minerals possessing lower ionic porosities tend to have smaller diffusivities and higher activation energies for diffusion. Since Pb is a charged species moving on lattice sites, such trends cannot be precise predictors of diffusion behavior or parameters (as Dahl also notes). However, the pyroxene data reported here do seem consistent with this observed correlation. Diopside has an ionic porosity of 33.4 (Dahl, 1997), the MBB clinopyroxene has a value of 34.2 (assuming a composition of $\sim Di_{40}Hd_{60}$, neglecting the small Johannsenite component), while the augitic pyroxene has an intermediate value ($\sim$ 33.7). Enstatite has the lowest ionic porosity of the investigated pyroxenes (33.2; Dahl, 1997). Higher values for this parameter indicate a more open mineral structure, so one would expect faster Pb transport in the more Fe-rich pyroxenes, and slowest transport in the enstatite, as is evident in the Pb diffusion data presented here.

5.2. Comments on the potential influence of early partial melting (EPM) on cation diffusion

It has been observed (e.g., Doukhan et al., 1993; Ingrin et al., 1991) that at temperatures well below their nominal melting temperatures, Fe-bearing pyroxenes exsolve a silica-enriched melt phase, a phenomenon termed early partial melting (EPM). Jaoul and Raterron (1994) argue that EPM, which appears to be related to cation vacancies associated with Fe^{+3} impurities, is a function of the Fe content of pyroxene and ambient fO_2, with the temperature of the onset of EPM falling with increasing percentage of Fe in the material. Ca diffusion in clinopyroxene (Dimanov et al., 1996) has been reported to depend on fO_2 when EPM is absent, and appears fO_2-independent when EPM is observed. However, there is little compelling evidence of dramatic change in activation energy for Ca diffusion in natural diopside at temperatures at which the onset of EPM is observed (i.e., $\sim$ 1130°C). Moreover, EPM is unlikely to have great effect on cation diffusion since the precipitates are isolated and do not form an interconnected network that would provide fast diffusion paths (e.g., Van Orman et al., 1998a). Lastly, the temperature range over which Pb diffusion is investigated in the present study is below the temperatures at which the onset of EPM is expected (e.g., Dimanov et al., 1996).

5.3. Effects of fO_2 on diffusion

As noted in an earlier section, there is a positive correlation between fO_2 and Pb diffusion rates for all of the investigated pyroxenes (Table 4; Fig. 6). Point defect models can be examined in order to shed light on possible mechanisms controlling Pb diffusion in pyroxenes.

A point defect model for diopside has been developed by Jaoul and Raterron (1994). In this model, Mg vacancies, Si vacancies, and Fe^{3+} are taken as the majority point defects. The diopside formula is written as $MeSiO_3$ (i.e., Me^{+2} is Ca^{+2} or Mg^{+2}), with no distinction made between M1 and M2 sites; the only substitution considered is Fe substituting for Me in either $+3$ or $+2$ charge state.

$$6Fe^{x}_{Me} + \frac{3}{2}O_2(g) \Leftrightarrow 3O^{x}_{O} + V''_{Me} + V''''_{Si} + 6Fe^{\bullet}_{Me}$$

The mass action law is then written as

$$[V''_{Me}][V''''_{Si}][Fe^{\bullet}_{Me}]^6 = K\, x^6 pO_2^{3/2}$$

where

$$x = [Fe^{x}_{Me}] = Fe/(Ca + Mg + Fe)$$

with the electroneutrality condition

$$2[V''_{Me}] + 4[V''''_{Si}] = [Fe^{\bullet}_{Me}]$$

applied.

For two-phase (Diopside-oxygen) equilibrium, anionic to cationic nonstoichiometry η is

$$\eta = \left(\frac{9x^6}{4^7}\right)^{1/8} pO_2^{3/16} K^{1/8}$$

and at constant T and P, the concentration of Me vacancies can be expressed as

$$[V''_{Me}] \propto [V''''_{Si}] \propto [Fe^{\bullet}_{Me}] \propto pO_2^{3/16}$$

The exponent $m = +3/16$ ($= 0.188$) derived from this model is quite similar to the dependence on pO_2 noted for Cr diopside and the DeKalb diopside (~ 0.5 at.% Fe), and does not differ greatly from the dependence noted for the augite and MBB cpx, despite notable compositional differences (especially in Fe content), or from the dependence exhibited by the enstatite. In all cases, the dependence is positive, suggesting a vacancy-controlled (octahedrally coordinated vacancies) mechanism for Pb diffusion in pyroxene. This is in contrast to the finding of Dimanov et al. (1996) in which a negative dependence on pO_2 was determined for Ca self-diffusion in natural Fe bearing (~ 2 at.% Fe) diopside, suggesting diffusion controlled by an interstitial mechanism. Possible reasons for this discrepancy are considered in the following section.

5.4. Comparison with diffusion rates of other cations in pyroxene

Fig. 9 is a plot of diffusion relations for various elements in both synthetic and natural pyroxenes. We first consider how the Pb data compare with diffusion rates for other divalent cations.

Mg diffusion in enstatite (Schwandt et al., 1998) is about 3–4 orders of magnitude faster than Pb diffusion in enstatite (for systems buffered at IW), although the activation energies for diffusion of Pb

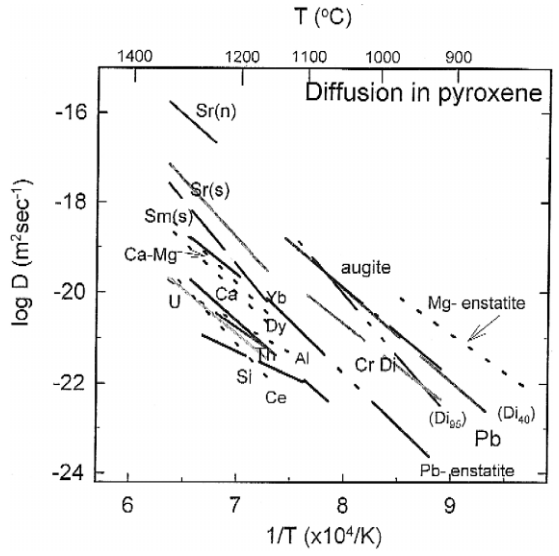

Fig. 9. Summary of measurements of cation diffusion in pyroxenes. Sources for data: Sr(n), Sr(s), Sm(s) [(n) natural, (s) synthetic diopside]—Sneeringer et al. (1984); Yb, Dy, Ce in diopside—Van Orman et al. (1998b); U, Th in diopside—Van Orman et al. (1998a); Al in diopside—Sautter et al. (1987), Jaoul et al. (1991); Si in diopside—Béjina and Jaoul (1996); Ca in diopside—Dimanov et al. (1996); Ca–Mg interdiffusion—Brady and McCallister (1983); Mg in enstatite—Schwandt et al. (1998); Pb in Di_{95}, Di_{40}—Cherniak (1998a); Pb in enstatite, augite, Cr diopside—this study.

and Mg normal to c are similar. However, the Mg diffusion experiments were run on an enstatite with higher Fe content ($En_{88}Fs_{12}$) than that used in the present work. Diffusion data from both this and earlier studies (e.g., Dimanov et al., 1996; Cherniak, 1998a) suggest, as noted earlier, that diffusivities might be somewhat higher in more iron-rich pyroxenes. However, the large differences in ionic radii between the divalent cations Mg and Pb (i.e., 0.89 and 1.29 Å for Mg and Pb, respectively; Shannon, 1976), probably account to greater extent for these differences in diffusion rates. Marked differences in diffusion rates among trivalent rare earth elements have been noted for both diopside (Van Orman et al., 1998b) and zircon (Cherniak et al., 1997a), with diffusion coefficients systematically increasing with decreasing REE ionic radius, with similar trends noted for divalent and univalent cations in plagioclase (Giletti and Shanahan, 1997; LaTourette and Wasserburg, 1998).

In contrast to Mg diffusion alone, Ca–Mg interdiffusion rates, obtained through homogenization of pigeonite lamellae in diopside (Brady and McCallister, 1983), lie near an up-temperature extrapolation of the Arrhenius relation for Pb diffusion in enstatite, and are about an order of magnitude slower than Pb diffusion in the Cr diopside. This observation is consistent with a diffusion process governed by exchange of Pb on Mg sites, with the large size differentials between Mg and Pb (and between Ca and Mg [1.29, 1.12, and 0.89 Å in eightfold coordination for Pb, Ca and Mg, respectively; Shannon, 1976]), a factor contributing to sluggish diffusion. The authors note that actual Ca–Mg interdiffusion coefficients could vary by as much as an order of magnitude due to the large thermodynamic effect on diffusion near a solvus, but the degree of agreement is encouraging nonetheless.

Ca self-diffusion (Dimanov et al., 1996) in natural Fe-bearing diopside, however, is considerably slower than diffusion rates of other divalent cations (including Sr, Sneeringer et al., 1984). Diffusion is about two orders of magnitude slower than Pb transport in the Cr diopside and DeKalb diopside. Based on point defect models and the fO_2 dependence of Ca diffusion they observe (i.e., increasing diffusion rates with decreasing fO_2), Dimanov et al. (1996) advocate an interstitial mechanism for Ca transport. It was noted earlier that the fO_2 dependence we find for Pb diffusion in diopside is in the opposite sense (i.e., increasing diffusion rates with increasing fO_2). It remains unclear why these differences, in both fO_2 dependence on diffusion and in relative rates of cation diffusion, exist.

It seems unlikely that Pb and Sr, much larger cations (0.17 and 0.14 Å larger than Ca in eightfold coordination, respectively; Shannon, 1976), would be able to move through the lattice by an interstitial mechanism, so this could explain the different fO_2 dependencies for Pb and Ca diffusion in clinopyroxene. Perhaps, movement via the interstitial mechanism also accounts for the slower diffusion rate for Ca with respect to Pb and Sr; if these species traveled via a similar diffusion mechanism, it might be expected that Ca would diffuse more rapidly than both given its smaller size.

Dimanov et al. (1996) report an activation energy of 396 ± 38 kJ mol^{-1} for temperatures above $\sim$ 1150°C, and 264 ± 33 kJ mol^{-1} for temperatures below 1150°C. They argue that the cutoff point between the two regimes represents the temperature of the onset of EPM, but the evidence for two distinct activation energies for Ca diffusion in natural diopside is, as was noted earlier, not robust. A fit to their Ca diffusion data over the entire temperature range would yield an activation energy for diffusion similar to those we have measured for Pb in the Cr diopside, but there is no reason to expect activation energies for diffusion to be comparable if Pb and Ca do indeed diffuse via different mechanisms.

The data for the DeKalb and Cr diopsides fall between down-temperature extrapolations from the diffusion data for Sr in natural and synthetic diopsides reported by Sneeringer et al. (1984). In their study, diffusivities for synthetic (with low Fe content) and natural (1.5 wt.% Fe) diopsides differed by two orders of magnitude. The natural specimens were annealed in nitrogen, while the synthetic specimens were annealed in air. The nitrogen atmosphere fixes the specimens at a constant (but unknown) oxygen fugacity, which the authors argue is probably higher than the ambient fO_2 conditions during crystal formation. Thus, oxidation of Fe and formation of vacancies would result from the anneal of the natural specimens under these conditions. We have already seen that diffusivities of cations in diopside and other pyroxenes increase with increasing Fe content (Dimanov et al., 1996; Cherniak, 1998a). The natural diopside contains at least eight times as much Fe as the synthetic diopside, so its higher diffusion rate is not inconsistent with these observations. For a comparable difference in Fe content, Ca diffusivities, using the findings of Dimanov et al. (1996), would differ by about a factor of seven (given a fixed pO_2 of 10^{-11} atm), but still well short of two orders of magnitude.

The findings we report here suggest a positive dependence of diffusion on fO_2 for large divalent cations in diopside. If we consider the annealing conditions for the natural diopside in Sneeringer et al.'s (1984) study to be oxidizing, and "normalize" the data to lower fO_2 conditions using the dependence of D on fO_2 derived for Pb diffusion in diopside (i.e., $m = 0.19$), we obtain the family of curves shown in Fig. 10 for MH, QFM, and IW. An up-temperature extrapolation from the Cr diopside

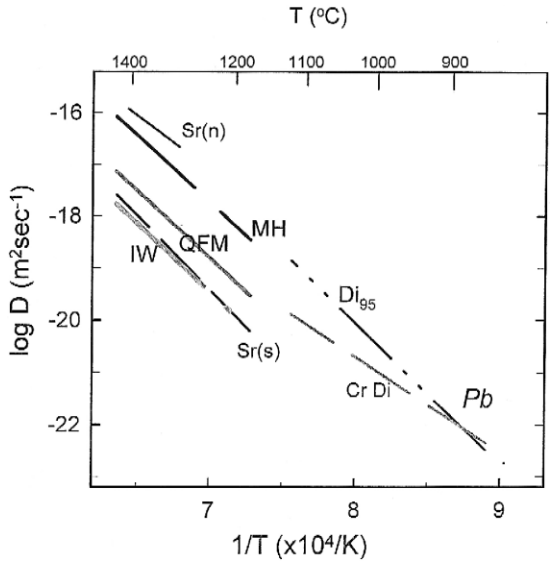

Fig. 10. Comparison of Pb diffusion rates in diopside with the findings for Sr diffusion in synthetic (s) low-Fe and natural (n) diopside by Sneeringer et al. (1984). The thick lines are calculations of "normalized" diffusion coefficients for Fe-bearing diopside at various fO_2 conditions (IW, QFM, and MH) based on the fO_2 dependence for diffusion of divalent cations determined in the present work. This normalization of the Sr diffusion coefficients for natural diopside to QFM conditions brings the data into better agreement with the Pb diffusion measurements (buffered at QFM), an agreement consistent with expectations for diffusion rates based on the similarity of the ionic radii of Sr and Pb.

data (experiments buffered at QFM) intersects the calculated QFM line. The DeKalb diopside line would lie somewhat above this (near MH) by virtue of the very high activation energy (544 ± 40 kJ mol^{-1}, similar to the activation energy for Sr diffusion in the synthetic diopside [548 kJ mol^{-1} for the RBS-measured profiles of Sneeringer et al., 1984]). Interestingly, the calculated line for the most reducing conditions (i.e., IW) is nearly coincident with the line for Sr diffusion in the synthetic diopside. This agreement may be merely fortuitous, but perhaps it indicates that a dominant factor influencing diffusion in pyroxenes is the change in defect chemistry (i.e., an increased vacancy concentration associated with electron holes needed to charge balance Fe^{+3}; e.g., Buening and Buseck, 1973) as a consequence of the oxidation of Fe.

Since ionic radii of Sr and Pb do not differ significantly (i.e., 1.29 Å for Pb and 1.26 Å for Sr in eightfold coordination; Shannon, 1976), similarities between Sr and Pb diffusion rates are unsurprising. Studies of Sr and Pb diffusion in feldspars (Cherniak and Watson, 1992, 1994; Cherniak, 1995a) have also evinced comparable diffusivities for these cations.

Diffusion of cations with higher valence states is slower than that of Pb in pyroxene. The tetravalent cations U and Th (Van Orman et al., 1998a), which likely substitute for Ca on M2 sites, diffuse several orders of magnitude more slowly than Pb. The trivalent REE (Van Orman et al., 1998b), and especially the LREE with large ionic radii, diffuse more slowly than Pb. Pronounced decreases in diffusivities with higher cation charge have been noted in the feldspars (e.g., Giletti and Shanahan, 1997; Giletti and Casserly, 1994; Cherniak and Watson, 1992, 1994; Foland, 1974), zircon (Cherniak et al., 1997a,b), and calcite (Cherniak, 1997, 1998b). Silicon diffusion is also quite sluggish in diopside (Béjina and Jaoul, 1996), consistent with observations made in other minerals, including olivine (Houlier et al., 1990), quartz (Jaoul et al., 1995; Cherniak, 1995b; Béjina and Jaoul, 1996), and anorthite (Cherniak, 1995b). However, the activation energy for Si diffusion in diopside is relatively low (211 kJ mol^{-1}) when compared with activation energies for diffusion of other cations. Al diffusion in diopside at 1 atm (Sautter et al., 1987; Jaoul et al., 1991) is also comparatively slow.

5.5. Pb diffusion in minerals: a consideration of some trends

Fig. 11 presents a summary of extant data for diffusion of Pb in minerals. Dahl (1997) has reported correlation of diffusion parameters (activation energies and pre-exponential factors), Pb diffusivities at a constant T (750°C), and Pb closure temperatures with mineral ionic porosities, and the results obtained here are consistent with these trends. In addition, there appear to be correlations of diffusion parameters with mineral elastic properties, as discussed in Cherniak (1998a). Minerals with larger Young's moduli generally exhibit larger activation energies (and pre-exponential factors), and consequently lower Pb diffusivities. These trends have also been noted (albeit for a much smaller data set)

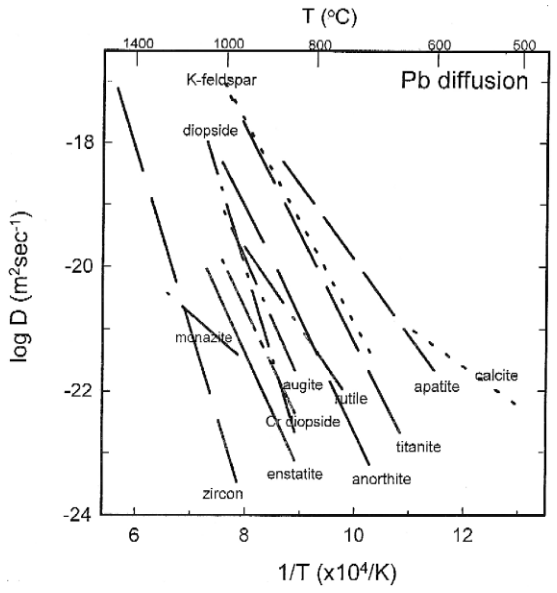

Fig. 11. Summary of Pb diffusion data for minerals. Sources for data: zircon—Cherniak and Watson (2000); monazite—Smith and Giletti (1997); rutile—Cherniak (2000); anorthite, K-feldspar—Cherniak (1995a); titanite—Cherniak (1993); apatite—Cherniak et al. (1991); calcite—Cherniak (1997); diopside (Di_{95}), buffered at QFM—Cherniak (1998a); augite, Cr diopside, enstatite (all buffered at QFM)—this study. Pb diffusion rates in pyroxenes are among the slowest in minerals for which diffusion data exist.

for REE diffusion (Cherniak, 1998b). Blundy and Wood (1991) have noted differences in partitioning behavior in plagioclase corresponding to variations in mineral elastic parameters, where the more flexible sodic plagioclase structure accommodates Sr and Ba ions more readily than does the more rigid calcic plagioclase. They have further extended these arguments and developed a predictive model (Blundy and Wood, 1994) to estimate partition coefficients as functions of Young's Moduli and cation size and charge. Similar reasoning might be applied to diffusional behavior if we conjecture that a more flexible (i.e., smaller elastic modulus) structure would also permit easier cation migration. Clearly, however, such simple correlations provide only first-order information (at best), as they do not account for defect structures that may influence diffusion, or consider the further complexities of the exchange process when additional charge-compensating species are involved. It should be noted, for example, that the minerals that most deviate from these trends (monazite, rutile, and K-feldspar) are those that would require movement of a charge compensating species along with Pb. In most of the other minerals (zircon excepted), it is most likely that there would be direct exchange of Pb for other divalent cations. More diffusion data on Pb are warranted in order to elucidate these systematic behaviors should they broadly exist.

6. Geological applications

6.1. Pb closure temperatures

Closure temperatures for Pb in the clinopyroxene compositions investigated can be calculated using the formalism of Dodson (1973) and the diffusion parameters reported here. However, it should be noted that the derivation of this familiar expression rests on several assumptions (Dodson, 1973, 1986); among these is the condition that the initial homogeneous composition of the mineral grain attained at peak temperature T_0 is sufficiently removed from the composition (at all points) of the quenched grain. This assumption, which makes T_c independent of T_0, is, as Ganguly and Tirone (1999) note, not satisfied for slowly diffusing species such as the REEs in garnet and various cations in pyroxene. However, when the dependence of T_c on T_0 is taken into account in calculating closure temperatures, the deviations of these T_c values from conventional closure temperatures calculated using the well-known Dodson equation, i.e.,

$$T_c = \frac{E_a/R}{\ln\left(\frac{ART_c^2 D_0/a^2}{E_a \mathrm{d}T/\mathrm{d}t}\right)}$$

are smaller with increasing peak temperature (T_0) and slower cooling rate (Ganguly and Tirone, 1999). The geometric factor, A, in Dodson's expression of mean closure temperature above, is equal to $\exp(G)$, where G is the value of the closure function, $G(x)$, spatially averaged over the crystal. In deriving the expression for $G(x)$, and ultimately A, the dimensionless parameter M [where M is defined as

$D(T_0)RT^2/(E_a a^2 \mathrm{d}T/\mathrm{d}t)$], is much greater than 1 (Dodson, 1986). For smaller values of M, the value of the closure function will increase, and thus the geometric factor will be greater than the value of 55 [i.e., exp (4.0066)] one obtains when the condition of $M \gg 1$ is met. The closure temperature will depart from Dodson's (1973) classical formulation, becoming lower with decreasing M.

Closure temperatures calculated using the expression above are mean values, as closure temperature varies with distance from the crystal surface. However, except for a very narrow outermost layer, closure temperatures will not differ from the mean by more than a few tens of degrees for cooling rates between 1 and 10°C/Ma and grain sizes up to a few millimeters. For example, for 100 μm radius grains, mean T_c is about 10°C higher than that for a point 10 μm from the surface; T_c for the grain center will be about 40°C higher than the mean value. A point 1 μm from the surface, however, will have a T_c 80–90°C lower than the mean.

It should be clear from this brief discussion that closure temperature is dependent on many factors. Beyond those already mentioned, closure temperature will also be a function of the effective diffusion radii of minerals and their modal abundance. Nonetheless, we can use the simplified expression above to make broad comparisons of conditions for closure to diffusion of Pb in pyroxenes to those for various accessory and more common minerals.

In simple closure temperature calculations, spherical geometry is assumed since our measurements suggest little anisotropy for Pb diffusion in the pyroxenes studied. Diffusion parameters for systems buffered at QFM are used in the calculations. Closure temperatures are plotted in Fig. 12 as a function of effective diffusion radius given a cooling rate of 10°C Ma^{-1}. Also plotted in the figure are closure temperatures for Pb in several other minerals for which diffusion data exist. Pyroxenes have comparatively high Pb closure temperatures. Calculated closure temperatures for pyroxene grains of 100 μm effective diffusion radius range from 725°C (Di_{40}) to 815°C (enstatite). Most other minerals close to Pb diffusional exchange at considerably lower temperatures. Considering a 100 μm effective diffusion radius, monazite (using the Pb diffusion data of Smith and Giletti, 1997), anorthite, titanite, K-feldspar, apatite and calcite closure temperatures are about 110°C, 120°C, 185°C, 200°C, 300°C, and 420°C lower than Cr diopside, respectively. Zircon is among the few minerals to have higher Pb closure temperatures than pyroxene. Based on the measurements of Cherniak and Watson (2000), Pb closure temperature in crystalline zircon is about 990°C for an effective diffusion radius of 100 μm and cooling rates of 10°C Ma^{-1}, a finding consistent with field-based estimates that indicate zircon closure temperature may be in excess of 900°C (Mezger et al., 1991; Mezger, 1994).

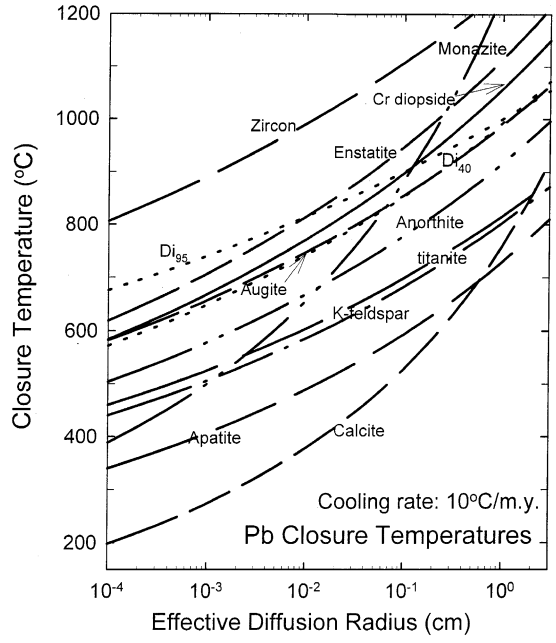

Fig. 12. Closure temperatures for Pb in several minerals as a function of effective diffusion radius. Values are calculated using Dodson's (1973) equation and the diffusion parameters from the data presented in Fig. 11. Given their relatively low diffusion rates for Pb, pyroxenes will close to Pb exchange at significantly higher temperatures than most minerals, with the exceptions of zircon and monazite.

6.2. Pb isotopic equilibration

The Pb diffusion data, and those from our earlier work (Cherniak, 1998a,b), permit a determination of the extent to which pyroxene grains will isotopically equilibrate with their external environments during a thermal event. We consider a simple model in which pyroxene grains are spheres with radii a and initial

uniform concentration of C_1, and are exposed to a medium with concentration C_0. The solution to the diffusion equation at the center of the spheres can then be derived (e.g., Crank, 1975) given these conditions. When the dimensionless parameter Dt/a^2 (where D is the diffusion coefficient and t is the time) is less than or equal to 0.03, the concentration at the center of the sphere remains unchanged from its initial value. Above 0.03, the concentration at the center of the sphere is affected by the externally imposed concentration C_0.

In Fig. 13 we plot curves representing $Dt/a^2 = 0.03$ for the pyroxene compositions investigated in this study, and those in Cherniak (1998a), given a 1 mm effective diffusion radius and systems buffered at QFM. Also plotted for comparison are curves for Sr equilibration in synthetic and natural diopside

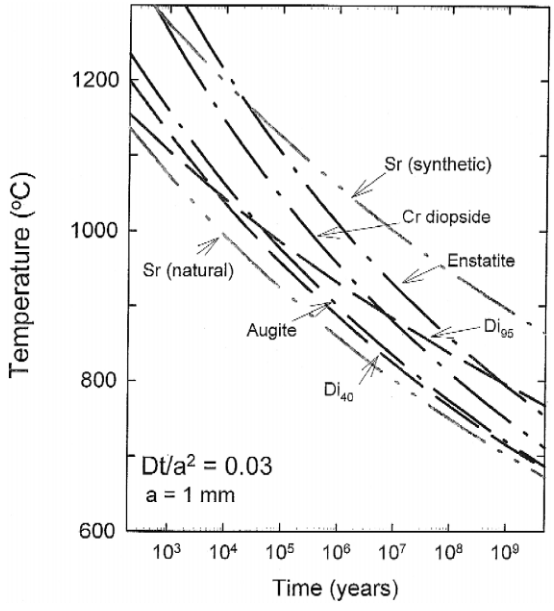

Fig. 13. Preservation of Pb compositions in pyroxene grains subjected to isothermal heating events. Curves represent maximum time–temperature conditions under which grains of 1 mm effective radius will preserve an initial Pb isotopic or chemical signature. When conditions above the curves prevail, this information will be lost through diffusional exchange. It will be retained under time–temperature conditions beneath the curves. Enstatite and diopside with low iron content are more resistant to diffusional alteration than clinopyroxenes of higher Fe content. Curves for Sr, calculated using the diffusion parameters in Sneeringer et al. (1984) for synthetic (with very low Fe concentrations) and natural diopside, bracket the curves for Pb.

derived from the Arrhenius parameters of Sneeringer et al. (1984). These curves define the time-temperature limits under which Pb (and Sr) isotopic information will be retained. For times and temperatures below the curves, Pb isotopic ratios at crystal cores will remain unaffected, but will be influenced by external Pb isotopic ratios when conditions above the curves exist. Low Fe diopside crystals of 1 mm effective diffusion radius will retain initial Pb isotopic ratios when heated at 800°C for times up to a few hundred million years, or at 900°C for up to a few million years. In more iron-rich clinopyroxenes, maximum time-temperature conditions under which Pb isotopic information is retained would be a few tens of million years at 800°C, and about 1 Ma at 900°C. Enstatite is more resistant to diffusional alteration, as information would be retained for >500 Ma at 800°C and >20 Ma at 900°C. Pb isotopic information would be preserved for times in excess of the age of the earth in Fe-rich clinopyroxenes at temperatures approaching 700°C, and temperatures about 750°C for low-Fe diopsides and enstatite. It should be stressed, however, that this simple model only considers alteration of Pb isotopes through volume diffusion. Other processes occurring in nature, such as recrystallization, may alter Pb isotopic and chemical compositions of pyroxenes on much shorter time scales.

The conditions necessary to alter Sr isotopes in synthetic and natural diopside bracket the curves calculated for Pb, with the synthetic diopside, because of its slower diffusion rates, more resistant to alteration. However, since diopsides with Fe contents as low as that found in the synthetic sample are comparatively rare in nature, the curve for synthetic diopside likely represents an upper limit of time-temperature conditions necessary for alteration of Sr isotopes, which may also be applicable for exchange under extremely reducing conditions.

Acknowledgements

I am grateful to Bruce Watson for invaluable discussion and advice throughout the course of this work. Jim van Orman, Tim Grove and Steve Mackwell offered insightful comments on diffusion in pyroxenes and other matters kinetic. Thoughtful re-

view comments from John Brady and Peter Dahl are sincerely appreciated. I thank Kiera Becker for assistance with electron microprobe analyses. I also thank the Mineralogical Museum at Harvard University for the enstatite (specimen #131539), and the Smithsonian's National Museum of Natural History for the augitic pyroxene (specimen #R15162-1), and greatly appreciate the assistance of Carl Francis and Paul Pohwat in selecting and sending mineral specimens from their respective institutions. This work was supported by grant EAR-9804794 from the National Science Foundation (to E.B. Watson).

References

Béjina, F., Jaoul, O., 1996. Silicon self-diffusion in quartz and diopside measured by nuclear micro-analysis methods. Phys. Earth Planet. Inter. 97, 145–162.

Blundy, J.D., Wood, B.J., 1991. Crystal–chemical controls on the partitioning of Sr and Ba between plagioclase feldspar, silicate melts, and hydrothermal solutions. Geochim. Cosmochim. Acta 55, 193–210.

Blundy, J., Wood, B., 1994. Prediction of crystal-melt partition coefficients from elastic moduli. Nature 372, 452–454.

Brady, J.B., McCallister, R.H., 1983. Diffusion data for clinopyroxenes from homogenization and self-diffusion experiments. Am. Mineral. 68, 95–105.

Buening, D.K., Buseck, P.R., 1973. Fe–Mg lattice diffusion in olivine. J. Geophys. Res. 78, 6852–6862.

Cherniak, D.J., 1993. Lead diffusion in titanite and preliminary results on the effects of radiation damage on Pb transport. Chem. Geol. 110, 177–194.

Cherniak, D.J., 1995a. Diffusion of lead in plagioclase and K-feldspar: an investigation using Rutherford Backscattering and resonant nuclear reaction analysis. Contrib. Mineral. Petrol. 120, 358–371.

Cherniak, D.J., 1995b. Si self-diffusion in feldspar. Eos Trans. AGU 76 (17), S299, Spring Mtg. Suppl.

Cherniak, D.J., 1997. An experimental study of Sr and Pb diffusion in calcite, and implications for carbonate diagenesis and metamorphism. Geochim. Cosmochim. Acta 61, 4173–4179.

Cherniak, D.J., 1998a. Pb diffusion in clinopyroxene. Chem. Geol. 150, 105–117.

Cherniak, D.J., 1998b. REE diffusion in calcite. Earth Planet. Sci. Lett. 160, 273–287.

Cherniak, D.J., 2000. Pb diffusion in rutile. Contrib. Mineral. Petrol. 139, 198–207.

Cherniak, D.J., Watson, E.B., 1992. A study of strontium diffusion in K-feldspar, Na–K feldspar and anorthite using ion implantation and Rutherford backscattering spectroscopy. Earth Planet. Sci. Lett. 113, 411–425.

Cherniak, D.J., Watson, E.B., 1994. A study of strontium diffusion in plagioclase using Rutherford Backscattering spectroscopy. Geochim. Cosmochim. Acta 58, 5179–5190.

Cherniak, D.J., Watson, E.B., 2000. Pb diffusion in zircon. Chem. Geol. In press.

Cherniak, D.J., Lanford, W.A., Ryerson, F.J., 1991. Lead diffusion in apatite and zircon using ion implantation and Rutherford Backscattering techniques. Geochim. Cosmochim. Acta 55, 1663–1673.

Cherniak, D.J., Hanchar, J.M., Watson, E.B., 1997a. Rare earth diffusion in zircon. Chem. Geol. 134, 289–301.

Cherniak, D.J., Hanchar, J.M., Watson, E.B., 1997b. Tetravalent cation diffusion in zircon. Contrib. Mineral. Petrol. 127, 383–390.

Crank, J., 1975. The Mathematics of Diffusion. 2nd edn. Oxford.

Dahl, P.S., 1997. The crystal–chemical basis for differential retention of Pb among geochronometric silicates and phosphates. Earth Planet. Sci. Lett. 150, 277–290.

Dimanov, A., Ingrin, J., 1995. Premelting and high-temperature diffusion of calcium in synthetic diopside: an increase of the cation mobility. Phys. Chem. Mineral. 22, 437–442.

Dimanov, A., Jaoul, O., Sautter, V., 1996. Calcium self-diffusion in natural diopside single crystals. Geochim. Cosmochim. Acta 60, 4095–4106.

Dodson, M.H., 1973. Closure temperature in cooling geochronological and petrological systems. Contrib. Mineral. Petrol. 40, 259–274.

Dodson, M.H., 1986. Closure profiles in cooling systems. Mat. Sci. Forum 7, 145–154.

Doukhan, N., Doukhan, J.-C., Ingrin, J., Jaoul, O., Raterron, P., 1993. Early partial melting in pyroxenes. Am. Mineral. 78, 1246–1256.

Dowty, E., 1980. Crystal–chemical factors affecting the mobility of ions in minerals. Am. Mineral. 65, 174–182.

Foland, K.A., 1974. Alkali diffusion in orthoclase. In: Hofmann, A.W., Giletti, B.J., Yoder, H.S. jr., Yund, R.A. (Eds.), Geochemical Transport and Kinetics. Carnegie Institution of Washington, pp. 77–98.

Fortier, S.M., Giletti, B.J., 1989. An empirical model for predicting diffusion coefficients in silicate minerals. Science 245, 1481–1484.

Ganguly, J., Tirone, M., 1999. Diffusion closure temperature and age of a mineral with arbitrary extent of diffusion: theoretical formulation and applications. Earth Planet. Sci. Lett. 170, 131–140.

Giletti, B.J., Casserly, J.E.D., 1994. Sr diffusion kinetics in plagioclase feldspars. Geochim. Cosmochim. Acta 58, 3785–3793.

Giletti, B.J., Shanahan, T.M., 1997. Alkali diffusion in plagioclase feldspar. Chem. Geol. 139, 3–20.

Houlier, B., Cheraghmakani, M., Jaoul, O., 1990. Silicon diffusion in San Carlos olivine. Phys. Earth Planet. Inter. 62, 329–340.

Ingrin, J., Doukhan, N., Doukhan, J.-C., 1991. High-temperature deformation of diopside single crystal: 2. TEM investigation of the defect microstructures. J. Geophys. Res. 96, 14287–14297.

Jaoul, O., Raterron, P., 1994. High-temperature deformation of

diopside crystals: 3. Influence of pO_2 and SiO_2 precipitation. J. Geophys. Res. 99, 9423–9439.

Jaoul, O., Sautter, V., Abel, F., 1991. Nuclear microanalysis: a powerful tool for measuring low atomic diffusivity with mineralogical applications. In: Ganguly, J. (Ed.), Advances in Physical Geochemistry, Diffusion, Atomic Ordering, and Mass Transport: Selected Problems in Geochemistry, vol. 6. Springer-Verlag, Berlin, pp. 198–200.

Jaoul, O., Béjina, F., Élie, F., Abel, F., 1995. Silicon self-diffusion in quartz. Phys. Rev. Lett. 74, 2038–2041.

LaTourette, T., Wasserburg, G.J., 1998. Mg diffusion in anorthite: implications for the formation of early solar system planetisimals. Earth Planet. Sci. Lett. 158, 91–108.

Mezger, K., 1994. Geochronology and metamorphism. V.M. Goldschmidt Conference Abstracts, Min. Mag. 58A, 605–606.

Mezger, K., Rawnsley, C., Bohlen, S., Hanson, G., 1991. U–Pb garnet, sphene, monazite, and rutile ages: implications for the duration of high grade metamorphism and cooling histories, Adirondack Mountains, New York. J. Geol. 99, 415–428.

Sautter, V., Jaoul, O., Abel, F., 1987. Aluminum diffusion in diopside using the $^{27}Al(p,\gamma)\,^{28}Si$ nuclear reaction: preliminary results. Earth Planet. Sci Lett. 89, 109–114.

Schwandt, C.S., Cygan, R.T., Westrich, H.R., 1998. Magnesium self-diffusion in orthoenstatite. Contrib. Mineral. Petrol. 130, 390–396.

Shannon, R.D., 1976. Revised effective ionic radii and systematic studies of interatomic distances in halides and chalcogenides. Acta Cryst. A 32, 751–767.

Smith, H.A., Giletti, B.J., 1997. Lead diffusion in monazite. Geochim. Cosmochim. Acta 61, 1047–1055.

Sneeringer, M., Hart, S.R., Shimizu, N., 1984. Strontium and samarium diffusion in diopside. Geochim. Cosmochim. Acta 48, 1589–1608.

Van Orman, J.A., Grove, T.L., Shimizu, N., 1998a. Uranium and thorium diffusion in diopside. Earth Planet. Sci. Lett. 160, 505–519.

Van Orman, J.A., Grove, T.L., Shimizu, N., 1998b. Rare earth element diffusion in diopside and disequilibrium melting in the mantle. Eos Trans. AGU 79 (17), S371, Spring Mtg. Suppl.